Title

Ellipsometric study of the electronic structure of Ga1-xMnxAs and low-temperature GaAs

Journal

Physical Review B, 70(20)

ISSN

1098-0121

Authors

Burch, Kenneth S
Stephens, J
Kawakami, R K
et al.

Publication Date

2004-11-01

Peer reviewed

Ellipsometric study of the electronic structure of $Ga_{1-x}Mn_xAs$ and low-temperature GaAs

K. S. Burch,[1,*] J. Stephens,[2] R. K. Kawakami,[2,†] D. D. Awschalom,[2] and D. N. Basov[1]
[1]*Department of Physics, University of California, San Diego, California 92093-0319, USA*
[2]*Center for Spintronics and Quantum Computation, University of California, Santa Barbara, California 93106, USA*
(Received 13 April 2004; revised manuscript received 19 July 2004; published 15 November 2004)

We have measured the optical constants of $Ga_{1-x}Mn_xAs$ from 0.62 to 6 eV, using spectroscopic ellipsometry. The second derivatives of the dielectric function are examined through a critical point analysis, allowing us to inspect interband transitions from different points in $\vec{k}$ space. The evolution of the band structure over a broad doping range is determined. Specifically, the E_1 critical point shifts to higher energies with increased doping of Mn, while all other critical points appear unaffected. The evolution of the critical points results from the interplay between band-gap renormalization due to ionized impurities and *sp-d* hybridization of the Mn induced impurity band with GaAs valence and conductions bands.

DOI: 10.1103/PhysRevB.70.205208 PACS number(s): 78.20.Ci, 78.40.Fy, 75.50.Pp

I. INTRODUCTION

Semiconductors doped with magnetic impurities, generally referred to as diluted magnetic semiconductors (DMS), have produced great scientific and technological interest in recent years.[1] Such systems offer a promising opportunity to explore devices that simultaneously exploit the spin and charge degrees of freedom.[2] They also bring the challenge of understanding the physics involved in the coupling of local moments in *d* orbitals with *sp* extended states. One of the most widely studied DMS is $Ga_{1-x}Mn_xAs$, in part because GaAs is a well characterized semiconductor used in a variety of digital signal processing circuits, telecommunication systems, and optoelectronics. While there is general agreement that ferromagnetism in $Ga_{1-x}Mn_xAs$ is driven by a carrier mediated mechanism between the local moments (Mn $3d^5$ electrons) and the carriers (holes),[3] the evolution of the electronic structure with Mn doping as well as its role in the ferromagnetism is still under debate.

The controversy around the electronic structure of $Ga_{1-x}Mn_xAs$ generally centers around the position of the Fermi level. One scenario places the holes in the Mn induced impurity band,[4–6] while others place the Fermi level in an unperturbed GaAs valence band.[3,7,8] These differing viewpoints are in part driven by the early work of Ohno *et al.*, who showed the onset of ferromagnetic behavior in $Ga_{1-x}Mn_xAs$ is at or near the metal to insulator transition.[1] Additionally, optical absorption measurements established the formation of a Mn induced shallow acceptor level 110 meV above the valence band in paramagnetic GaAs doped with Mn in the very dilute limit.[9] Recent STS and ARPES experiments suggest the Mn forms an "impurity band" of *d*-like states that strongly hybridize with the GaAs valence band.[10–12] The ARPES measurements place the occupied d^5/d^4 levels ≈ 5.3 eV below the valence band maximum (VBM), with the unoccupied d^5/d^6 level lies 3.7 eV above the VBM (see Fig. 1).[12] Nonetheless these measurements are limited in resolution, and therefore the quantitative evolution of the band structure with *x* has yet to be established experimentally. Infrared spectroscopy measurements established the role of this impurity band in the carrier dynamics of $Ga_{1-x}Mn_xAs$, however they were limited to energies below the band gap and could only discuss effects at the zone center.[13,14]

Experimental studies of the $Ga_{1-x}Mn_xAs$ electronic structure that combine high resolution, broad doping range, and do not focus on the zone center are needed to address several key issues. Interestingly, although $Ga_{1-x}Mn_xAs$ is generally referred to as a "compound," implying the momentum ($\vec{k}$) is conserved and is still a good quantum number, this has yet to be confirmed experimentally. Additionally the effects on the GaAs band structure of *sp-d* hybridization between the Mn *d* and As/Ga *sp* states are still unknown. To investigate these and other effects of Mn doping we have a performed a line shape analysis of the complex dielectric function determined by spectroscopic ellipsometry.

For the past four decades, spectroscopic ellipsometry has provided key insights into the electronic structure of many materials.[15] Unlike common spectroscopic techniques, ellipsometry measures the amplitude and phase of the reflected wave. Therefore, the complex dielectric response $[\hat{\epsilon}(E)]$ of a

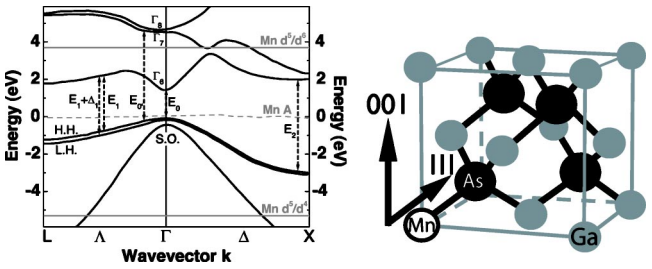

FIG. 1. Left: GaAs band structure and relevant critical point transitions reproduced from Ref. 24. The upper conduction bands are labeled as Γ_7 and Γ_8 based on symmetry, while the lowest conduction band is labeled Γ_6. The valence bands have been labeled as H.H. for heavy-hole, L.H. for light-hole, and S.O. for split-off. Taken from Ref. 12, Mn *d* filled (d^5/d^4) and empty (d^5/d^6) levels are shown in grey, and the acceptor Mn A is dashed-gray. The dispersion of the Mn acceptor level is also taken from Ref. 12. The L point corresponds to the 111 direction and the X point to the 001 direction. Right: $Ga_{1-x}Mn_xAs$ unit cell with the important symmetry directions labeled.

material can be obtained analytically in bulk isotropic materials. The optical constants of a layered structure can be determined with high resolution ($\approx$1 meV) over a broad energy range ($\approx$0.6–6 eV). Strong features in the spectra result from the enhanced interband transitions at points in the Brillouin zone where the slope of the two bands are nearly identical (see Fig. 1). An analysis of $d^2\hat{\epsilon}(E)/dE^2$ provides direct determination of the energy of these "critical points." This motivated us to perform an ellipsometric study of $Ga_{1-x}Mn_xAs$ such that a detailed view of the evolution of the band structure at a number of points in *k*-space can emerge. Similar efforts on II–VI DMS have aided in the determination of the strength of *sp-d* hybridization ($V_{(s,p)d}$) in these materials.[16] An understanding of the role of *sp-d* hybridization in DMS is critical, as a strong $V_{(s,p)d}$ can lead to the formation of a Zhang-Rice polaron, binding the Mn induced hole.[17] The strength of $V_{(s,p)d}$ will also determine the strength of the hopping amplitude "*t*" of the holes,[17,18] central to a number of different theories of ferromagnetism in $Ga_{1-x}Mn_xAs$.[4–6] Additionally, the kinetic exchange, which plays a large role in the magneto-optical properties of $Ga_{1-x}Mn_xAs$,[7] can be related to the *sp-d* hybridization via second order perturbation theory ($N_0\beta \propto V_{pd}^2$).[19] As discussed in Sec. IV A, *sp-d* hybridization will also result in *sp* bands avoiding the Mn *d* levels,[16,19–21] and is therefore central to understanding of the band structure in $Ga_{1-x}Mn_xAs$.

Our spectroscopic investigation has revealed the evolution of the band structure of Mn doped GaAs. Specifically, from the critical point analysis we uncover the important role of hybridization between Mn induced impurity band and the GaAs valence band. Namely the anisotropic strength of this hybridization results in a blueshift of the E_1 transition while all other critical points remain unchanged. This analysis is discussed in Sec. III C. The measured elipsometric data can be found in Sec. III A. The samples and experimental methods are described in Sec. II. The fitting procedure is described in the Appendix and the resulting dielectric function is detailed in Sec. III B. Finally we discuss the implications for each critical point in Sec. IV.

II. SAMPLES AND EXPERIMENTAL METHOD

The samples in this study were grown at the University of California, Santa Barbara on semi-insulating GaAs(100) by low temperature molecular beam epitaxy (LT-MBE). The $Ga_{1-x}Mn_xAs$ and LT-GaAs samples were deposited at a temperature of 260 °C. The sample labeled GaAs is a bare substrate. The $Ga_{1-x}Mn_xAs$ layers had a nominal thickness of 500 nm and were grown atop a 60 nm LT-GaAs buffer layer. The LT-GaAs sample had a nominal thickness of 1500 nm (see Fig. 7 for details). The oxide and buffer layers were taken into account using a multiphase analysis described in the Appendix.

Spectroscopic ellipsometry (0.62–6 eV) and near-normal incidence transmission (*T*) measurements over the energy range 0.005–1.42 eV were performed at the University of California, San Diego at room temperature. Details of the transmission measurements can be found in Ref. 13. For the ellipsometry experiments the back surface of the substrate was roughened so as to prevent interference in the substrate. A variable angle spectroscopic ellipsometer (VASE) instrument from J. A. Woollam and Associates with a rotating analyzer and an autocompensator measured the complex ellipsometric ratio (ρ) at 65° and 75° angle of incidence. ρ is the ratio of the reflectance coefficients r_p and r_s (parallel and perpendicular to the plane of incidence). This is generally expressed in terms of two angles Ψ and Δ:

$$\rho = \frac{r_p}{r_s} = e^{i\Delta} \tan \Psi, \tag{1}$$

where Ψ is a measure of the relative amplitude and Δ the relative phase shift. From Ψ and Δ the complex dielectric function $[\hat{\epsilon}(E) = \epsilon_1(E) + i\epsilon_2(E)]$ can be readily derived using the two-phase model (*ambient+sample*).[22] However, in real materials surface roughness, oxide overlayers and the multilayered nature of the samples require multiphase modeling (see Appendix), which results in genuine optical constants.[22] A significant parameter in evaluating these models is the penetration depth of the incident light (δ):

$$\delta = \frac{\lambda}{4\pi k}, \tag{2}$$

where λ is the wavelength of the incident light and *k* is the complex part of the index of refraction $[\sqrt{\hat{\epsilon}(E)} = \hat{n} = n + ik]$.[23] If a layer has a thickness greater than 2δ then layers below it do not contribute to the measured Ψ and Δ, because of strong attenuation.[24] Therefore in regions where $\epsilon_2(E)$ is large and/or at higher energies, the primary contribution is from the top few atomic layers. Specifically in the region of the E_1 critical point $\delta(E_1) \approx 20$ nm, whereas near E_2 $\delta(E_2) \approx 5$ nm.

III. RESULTS AND ANALYSIS

A. Ψ and Δ

In Fig. 2 we plot the measured ellipsometric parameters at 65° (top panels) and 75° (bottom panels) angle of incidence. We first take note of the significant difference in the shape and magnitude of Δ at these two angles. The uniqueness of the information garnered at the measured angles is the result of taking data just below and above the Brewster's angle for GaAs. Turning our attention to the low energy portion of the spectra ($E \leqslant 1.75$ eV), interference fringes appear in all samples except the bare substrate. In this range we approach the fundamental band gap of GaAs, which can be seen as sharp points around 1.42 eV in both Ψ and Δ. Furthermore, in this region *k* becomes sufficiently small and λ adequately long so that 2δ is greater than the thickness of the deposited film.[25]

We now examine the region between 2.5 and 3 eV. Focusing first on Ψ, we see that at both angles the GaAs data display two sharps points. These are the E_1 and $E_1+\Delta_1$ critical points that result from the almost parallel nature of the conduction and valence bands near the Λ point (see Fig. 1).

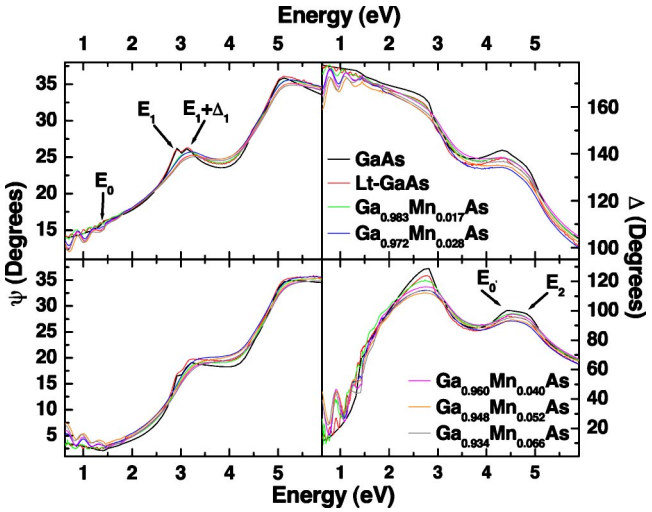

FIG. 2. Ellipsometric angles Ψ and Δ measured at a 65° (top panels) and 75° (bottom panels) angle of incidence. The interference fringes at low energies are due to interference from the thin film. The two peaks around 3 eV are due to the E_1 and $E_1+\Delta_1$ critical points, which clearly broaden and blueshift with Mn doping. However, Mn doping has little effect on the two extrema around 4.5 and 5 eV are due to the $E_{0'}$ and E_2 critical points.

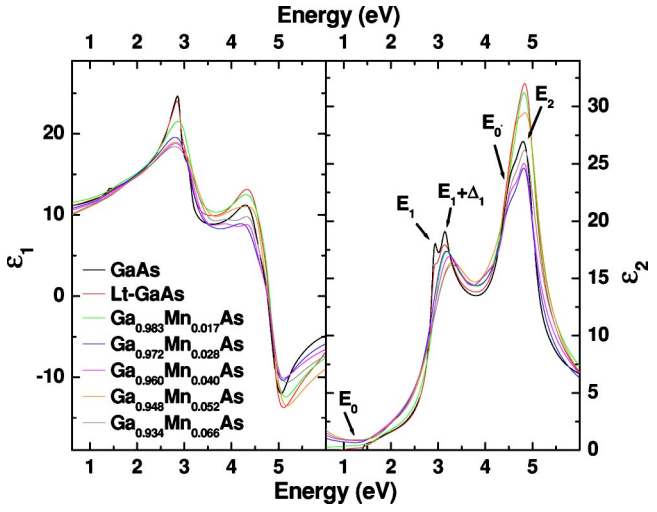

FIG. 3. Left panel: The real part of the dielectric function for all samples in this study. Right panel: The imaginary (absorptive) part of the dielectric function with the critical points labeled. In both panels we clearly see the broadening of E_0 and E_1 with Mn doping, while the right panel clearly demonstrates the blueshifting of E_1. We also note the apparent lack of change in $E_{0'}$ and E_2.

These critical points are broadened due to disorder in all the samples in this study. Due to this broadening, in $Ga_{1-x}Mn_xAs$ the two critical points appear to have merged. This trend can also be seen in the Δ data taken at 75° (see Fig. 2). In Fig. 2 we note a reduction in Ψ between 2.75 and 3 eV and concurrent growth below 2.5 eV.

Finally, we turn our attention to the region between 4 and 5 eV. While data in this region is affected by the native oxide layer, discussed further in Sec. IV E, there is an important trend worth noting. This is best seen in Δ at 75°, where two clear peaks are evident in the GaAs data. While the sharpness of the peaks appears reduced in the LT-GaAs and $Ga_{1-x}Mn_xAs$ samples, this does not seem to be the result of significant broadening. Most notably the position of these two peaks remains unchanged with Mn doping.

B. Optical constants

The $\hat{\epsilon}(E)$ spectra resulting from the modeling of Ψ and Δ, as described in the Appendix, are displayed in Fig. 3. The critical points of GaAs have been labeled in the graph of $\epsilon_2(E)$. Consistent with our earlier work on these samples, we find that the fundamental band gap (E_0) is significantly broadened in LT-GaAs and $Ga_{1-x}Mn_xAs$ samples such that a sharp onset is no longer observed.[13] We note that this effect can be seen in both $\epsilon_1(E)$ and $\epsilon_2(E)$. The origin of this broadening will be discussed in Sec. IV B, however Fig. 3 demonstrates that this broadening grows with Mn doping until $x=0.028$. Additionally this effect seems to extend to $\sim$2.75 eV. This band gap broadening is aided by a transfer of spectral weight from the region between 2.75 and 3.25 eV to the region below 2.75 eV.

We now discuss the region of the E_1 and $E_1+\Delta_1$ transitions, namely 2.5$\rightarrow$3.5 eV. First focusing on $\epsilon_1(E)$ we note that as we increase the doping the peak at 2.85 eV broadens and decreases in strength. Turning our attention to $\epsilon_2(E)$, the E_1 peak is broadened and decreases in strength in LT-GaAs. However in the Mn doped samples the E_1 peak can no longer be distinguished from the $E_1+\Delta_1$ critical point. It is interesting to note that previous studies of doped GaAs revealed a redshifting of both the E_1 and $E_1+\Delta_1$ transitions.[26] However, a blueshift in E_1 is observed in $Ga_{1-x}Mn_xAs$, while the broadening and reduction in amplitude are consistent with previous studies.[26]

Finally we turn our attention to the region of the $E_{0'}$ and E_2 critical points (4.25$\rightarrow$5.25 eV) in Fig. 3. These critical points result from transitions near the zone center and at the X point respectively (see Fig. 1). Despite the presence of the oxide layer and the small penetration depth ($\delta\approx 5$ nm), the critical points can still be clearly recognized in all $\epsilon_1(E)$ spectra and in most of the $\epsilon_2(E)$ spectra. Focusing on $\epsilon_1(E)$, we see that the position and broadening of the $E_{0'}$ and E_2 critical points appears almost constant throughout the series. Not surprisingly, the amplitude of this peak appears to be random, as previous ellipsometric studies established the effect of the oxide layer reduces the strength of the measured E_2 peak.[27] Therefore we do not expect the presence of the oxide layer to significantly effect our critical point analysis.

C. Critical point analysis

The numerical second derivatives of the $\hat{\epsilon}(E)$ data presented in Fig. 3 can be found in Fig. 4. A cursory examination of this graph reveals its utility in analyzing the structures seen in the $\hat{\epsilon}(E)$ spectra. Before discussing the results separately for each of the relevant critical points, we briefly mention some general trends in the data. The $E_{0'}$ and E_2 critical points, with the exception of the $Ga_{0.948}Mn_{0.052}As$ sample, appear almost completely unaffected by growth at low tem-

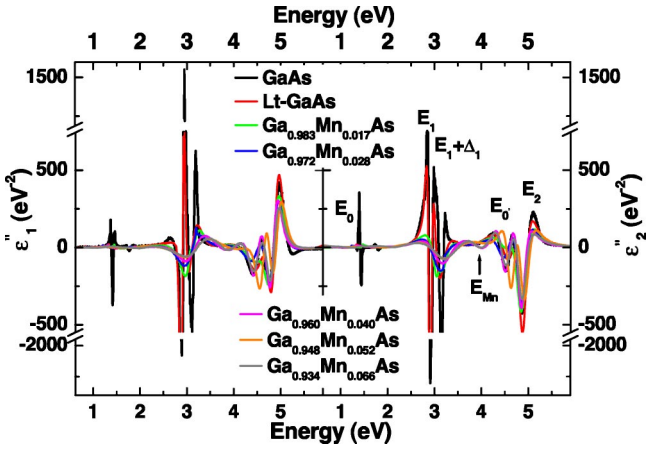

FIG. 4. Derivative spectra of all samples in this study, which allow a clear identification of all critical points. We note the complete loss of a feature at E_0 in all samples grown by low temperature MBE. The E_1 critical point is significantly broadened and blueshifted with Mn doping, while $E_{0'}$ and E_2 show little change.

perature and/or Mn doping. We believe the anomalous behavior of the $Ga_{0.948}Mn_{0.052}As$ sample results from having had the longest exposure to air (see Table I), however it's origin is not entirely clear. Interestingly for samples with $x \geqslant 0.04$, an extremely weak extra feature (labeled E_{Mn}) appears at energies just below $E_{0'}$. The origin of this peak will be discussed in Sec. IV D.

Next we turn our attention to the E_0 and $E_0+\Delta_0$ transitions, which undergo a substantial change attributable to the low temperature growth. Namely, these transitions are no longer observable in the $d^2\hat{\epsilon}(E)/dE^2$ spectra and therefore we have not attempted to fit these transitions in any sample, with the exception of the GaAs substrate. However, given the band edge broadening seen in Fig. 3, this result is not surprising.

Let us now examine the E_1 and $E_1+\Delta_1$ critical points, which contain rather surprising results. We begin by comparing LT-GaAs and GaAs, noting a significant reduction in the amplitude of the critical points in the former with respect to the later. However in LT-GaAs the broadening of the E_1 critical point appears unchanged by low-temperature growth

TABLE I. Parameters of the samples studied, which were grown at a substrate temperature of 265 °C, with As/Mn beam flux ratio of ~200/1. Ga growth rates were ~0.3 ML/s and Mn growth rates were 0.02–0.05 ML/s. All thicknesses are in nm and T_C are in Kelvin.

Sample	Surface layer	Oxide layer	Generic layer	T_C
GaAs	0.211	2.966	n.a.	n.a.
LT-GaAs	0.289	4.64	1558.5	n.a.
$Ga_{0.983}Mn_{0.017}As$	0.332	3.973	514.47	<5
$Ga_{0.072}Mn_{0.028}As$	0.846	3.317	480.17	30
$Ga_{0.060}Mn_{0.040}As$	0.848	2.533	485.47	45
$Ga_{0.048}Mn_{0.052}As$	0.918	4.075	479.57	70
$Ga_{0.034}Mn_{0.066}As$	0.88	3.138	497.96	70

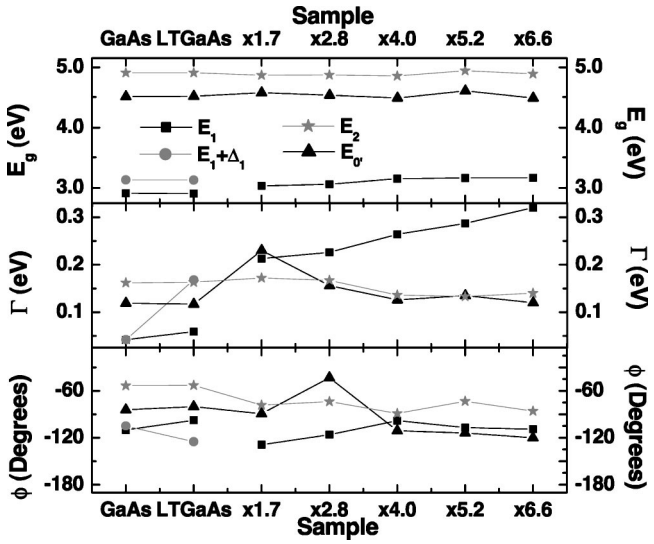

FIG. 5. (Top panel) The resonant energy of each critical point for all samples. We note the increase in E_1 with increasing x, while all other points remain unchanged. (Middle panel) The broadening of the critical points for each sample. The sudden change in the $x=1.7\%$ sample is due to the merging of E_1 and $E_1+\Delta_1$. (Bottom panel) The phenomenological phase parameter which accounts for the mixing of different critical points due to Coulomb effects. Lines are guides to the eyes. When the E_1 structure just overlaps the $E_{0'}$ critical point, it results in $E_{0'}$ appearing more asymmetric. We therefore conclude that the significant broadening and blueshifting of E_1 is responsible for the apparent anomalies at $x=0.017, 0.028$. In the samples with higher dopings, the amplitude of the E_1 critical point continues to be reduced and the overlap between E_1 and $E_{0'}$ increases, reducing the asymmetric effect of E_1 on $E_{0'}$.

while the $E_1+\Delta_1$ appears to be significantly broadened. As we expect from Fig. 3, the effect of Mn doping is quite dramatic. In all Mn doped samples, the broadening of the E_1 and $E_1+\Delta_1$ critical points is such that they appear to merge. Additionally this merged structure is continuously blueshifted as x is increased.

In GaAs at room temperature, the derivative spectra in the vicinity of a critical point are well characterized by two-dimensional line shapes:[27,28]

$$\frac{d^2\hat{\epsilon}(E)}{dE^2} = Ae^{i\Theta}(E - E_g + i\Gamma)^{-2}, \tag{3}$$

where A is the amplitude of the critical point related to the reduced effective mass of the two bands involved in the transition, E_g is the energy of the critical point, and Γ is a broadening parameter determined by the quasiparticle lifetime and the relaxation of the requirement of momentum conservation. The phenomenological parameter Θ is added to account for Coulomb and excitonic effects that result in the admixture of two critical points.[29]

The critical point parameters (E_g, Γ, Θ) determined by fitting the numerical second derivative to the form given in Eq. (3) are plotted in Fig. 5. The details of the fitting procedure can be found in the Appendix. Examining the gap energies

plotted in Fig. 5, we see that the fitting results are in reasonable agreement with our expectations from Figs. 2, 3, and 4. Specifically E_g of the E_1 critical point blueshifts with increasing Mn doping, while $E_{0'}$ and E_2 remain unchanged within experimental error. In Fig. 5, we also find that E_1 critical point is significantly broadened while the other critical points remain mostly unchanged by low-temperature growth.

IV. DISCUSSION

A. Perturbations of the critical point energies

The Hamiltonian of Mn doped GaAs contains two terms due to exchange (Coulomb) and hybridization (kinetic) between the Mn *d* orbitals and the As/Ga *sp* orbitals. The exchange term produces a redshift of the critical points,[16,30] yet only blueshifting, if any, is seen in our data. This results from the fact that at room temperature, $Ga_{1-x}Mn_xAs$ is paramagnetic, significantly reducing the effect of the exchange interaction. The effect of *sp-d* hybridization on the band-gap energies of DMS was first proposed in an ellipsometric study of $Cd_{1-x}Mn_xTe$, and has since been described theoretically[21] and observed experimentally in $Zn_{1-x}(Mn,Fe,Co)_xTe$[16] and $Ga_{1-x}Fe_xAs$.[31] Qualitatively the *s* and *p* bands of the host are repelled by the *d* levels through *sp-d* hybridization, such that if a *d* level is above(below) an *sp* band it pushes the *sp* band to lower(higher) energy. We note that due to symmetry considerations, hybridization has no effect on the Γ_6, *s*-like, conduction band at the Γ point. However, since this is a second order effect, the shifting is inversely proportional to the energy separating the s,p and *d* bands. Carefully examining Fig. 1, we expect the separation between the light hole, heavy hole, and split-off band to be strongly affected by *sp-d* hybridization.

Another term in the Hamiltonian arises from the perturbing potential of the impurities in the sample. This effect was first studied in Si[32] and later in Ge[33] and GaAs[28] and agrees well with the result of second-order perturbation theory. The impurities, acceptors, and/or donors, provide scattering centers such that the self energy is altered. The self energy of a particle in state $|\vec{k},n\rangle$ is perturbed by a second order process, whereby it scatters into a virtual intermediate state $|\vec{k}+\vec{q},n'\rangle$ and then back into the original state $|\vec{k},n\rangle$. This results in redshifting and broadening of the critical points.

If we assume Thomas–Fermi screening, to second order the changes in E_g can be written as

$$\Delta E_g^x = E_g^x - E_g^0 \approx \sum_q \frac{N_{\rm imp}}{(q^2+q_{\rm TF}^2)} - \sum_q \frac{N_{\rm imp}}{(q^2+q_{\rm TF}^2)^2} + x\sum_i \left(\frac{V_{(s,p)d}^2}{E^C - E_i^d} - \frac{V_{pd}^2}{E^V - E_i^d} \right) + \Delta E_{\rm strain}^x, \qquad (4)$$

where E_g^x is the value of the gap at *x* doping of Mn, $N_{\rm imp}$ is the impurity density, $E^{C,V}$ the energy of the conduction (valence) band involved in the transition, E_i^d the energy of the *i*th Mn level, and $q_{\rm TF}^2 \propto p^{1/3}m^*$ is the Thomas–Fermi wave vector with *p* the carrier concentration and m^* their effective mass. The first and second terms in Eq. (4) are the first- and second-order perturbations due to the impurity potentials.[28] The first term in Eq. (4) is generally small and has a different sign for acceptors and donors, such that in heavily compensated materials this term can be neglected. The second-order term produces redshifts proportional to $N_{\rm imp}^{\alpha}$, where $\alpha = 1(1/3)$ for large(small) *q* scattering where *q* is much greater(lesser) than $q_{\rm TF}$. For $Ga_{1-x}Mn_xAs$ the impurity density is quite large, we therefore expect large *q* scattering to dominate. The third term in Eq. (4) is the result of second-order perturbation theory of the *sp-d* hybridization.[19] Although not explicitly stated in Eq. (4), $V_{(s,p)d}$ has $\vec{k}$ dependence that results from the directional dependence of the overlap of *sp* and *d* orbitals. The fourth term, $\Delta E_{\rm strain}^x$ is the shift in the critical point energy due to compressive strain in the thin film. Since the lattice constant of $Ga_{1-x}Mn_xAs$ generally follows Vegard's law (grows linearly with *x*), the films will be under increasing compressive strain. As we will demonstrate in Sec. IV C, the strain results in a small redshift. Therefore the size of ΔE_g will depend on the direction and position in $\vec{k}$ space of the transition, m^*, *p*, and the density of ionized impurities.

B. E_0

The results presented in this paper provide additional insights into the broadening of the band gap of GaAs grown at low temperatures. In our previous studies of these samples we clearly established that this broadening was, in part, the result of transitions either beginning (in the case of *n*-type LT-GaAs) or ending (in the case of *p*-type $Ga_{1-x}Mn_xAs$) in the As_{Ga} impurity states.[13] However, with the additional information provided by the $\hat{\epsilon}(E>1.5\ \text{eV})$ we see that this broadening is also the result of a relaxation of the requirement of momentum conservation. As discussed in the previous section, this relaxation is due to the presence of impurities that provide additional scattering mechanisms. Since transitions are no longer required to be direct, states in the valence band that are not at the zone center can contribute to transitions which end at the zone center. Ultimately this results in a broadening of transitions and a transfer of spectral weight from higher energies to lower ones, as is seen in Fig. 3. We note that a similar result is found in GaAs damaged by ion implantation.[34]

C. E_1 and $E_1+\Delta_1$

The E_1 and $E_1+\Delta_1$ critical points result from the almost parallel nature of the heavy and light hole valence bands and the Γ_6 conduction band near the Λ point (see Fig. 1). The blue shifting of E_1 is quite surprising as these samples contain a large defect concentration. However, in LT-GaAs E_1 is unperturbed due to the nature of the defects in this sample, namely As_{Ga}. Since As_{Ga} are deep double donors (activation energy $\geqslant 0.5$ eV), their electrons are very efficient at screening the impurity potential, preventing As_{Ga} from effecting the band structure. Yet in $Ga_{1-x}Mn_xAs$, as *x* is increased the Fermi level moves closer to the valence band and the material first becomes fully compensated, then *p* type.[10,12,13,35,36]

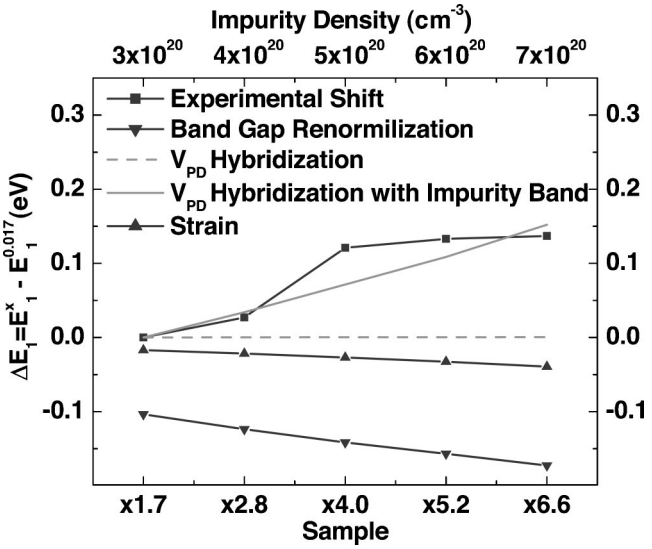

FIG. 6. The measured shift in E_1 with increasing x. The redshifts due to strain and band-gap renormalization are also plotted. The shift of E_1 resulting from hybridization between the sp and d levels are drawn in gray. The impurity band must clearly be included in the hybridization to explain the blue shift in E_1. Lines are guides to the eyes.

We therefore expect the screening of the potentials to be significantly reduced at low Mn dopings. Then as the number of carriers increases, the effect of the impurities on the band structure should be diminished. As a result the renormalization of the E_1 critical point will be substantial at low dopings, then flatten out or possibly be reduced as the number of carriers increases.

The significant blueshifting seen in these critical points suggests the impurity perturbations are overcome by a strong V_{pd} interaction occurring in the 111 direction. This result is not entirely surprising, given the strong hybridization believed to occur between Mn d and As p orbitals.[11,12,37] Additionally, regardless of the site of the substitutional Mn atom in the unit cell, it will always have As neighbors in the 111 and/or $\overline{111}$ directions (see Fig. 1). To qualitatively evaluate Eq. (4) for E_1, we must carefully consider the result of adding a $3d^5$ local moment to the GaAs environment. Examining Fig. 1 we see that the d levels are far in energy from the bands involved in the E_1 critical point, such that they would most likely cause a small redshift of this transition. However, the Mn acceptor level is just above the GaAs valence bands. Photoemission on $Ga_{1-x}Mn_xAs$ has demonstrated the d-like character of this level as well as its strong hybridization with the As $3p$ states.[12]

To quantitatively examine these trends, in Fig. 6 we have plotted $\Delta E_1^x = E_1^x - E_1^{0.017}$, where E_1^x is the measured position of the E_1 critical point at a given doping x. We have chosen to plot the shift this way to account for the merging of the E_1 and $E_1+\Delta_1$ critical points. Additionally the calculated shifts due to strain, ionized impurities, and pd hybridization are plotted separately in Fig. 6. It appears that hybridization between the Mn induced impurity band and the GaAs valence band is needed to fully account for the blueshifting. These results also suggest that the defects in $Ga_{1-x}Mn_xAs$ are well screened by the carriers, which may not be surprising due to their large effective mass ($0.5m_e < m^* < 2.5m_e$).[13,28] Furthermore, in previous ellipsometric studies of doped semiconductors, only one type of dopant was used, either acceptors or donors. However in $Ga_{1-x}Mn_xAs$ both acceptors and donors are present. Interestingly, previous investigations suggest that the positions of these defects will be correlated, such that they will tend to cluster.[38] Therefore, the effect of the impurity potentials may be reduced, as dipole fields are typically much weaker than single-ion potentials.

One alternate scenario that would explain the blue shifting of the E_1 critical point, involves reducing the separation between the GaAs conduction band and the d^5/d^6 level, such that it lied below the conduction band near the Λ point. While this would also result in a blueshifting of E_1, we believe this scenerio is highly unlikely, for two reasons. First, from a theoretical standpoint it would require a significant reduction in the onsite Coulomb repulsion U_{eff}, which seems highly suspect. Second, as discussed in the next section, in higher doped samples we observe evidence of a transition from the valence bands to the d^5/d^6 level, which agree with its placement from previous photoemission studies. We therefore conclude that the blueshifting of E_1 with Mn doping is the result of hybridization between the Mn impurity band and the GaAs valence band.

As discussed in Sec. IV A, the internal strain in $Ga_{1-x}Mn_xAs$ will also result in a redshift of the E_1 and $E_1+\Delta_1$ critical points. Using the lattice parameters established in Ref. 1 we have estimated the redshift in $E_1 \leqslant 0.019$ and $E_1+\Delta_1 \leqslant 0.013$ (see Fig. 6).[39] Additionally these samples are 500 nm thick and grown on 60 nm buffer layers such that the topmost layers of the films should be relaxed. In the vicinity of the E_1 critical point, δ is as long as 20 nm. We therefore conclude strain has little or no effect on measured critical point energies. This also suggests that the broadening of E_1 and $E_1+\Delta_1$ is not the result of a lifting of the degeneracy of the "z" component of angular momentum in the light and heavy hole valence bands. In particular, since $j_z = \pm 3/2$ the internal splitting due to strain is more significant for the heavy hole band, therefore the broadening of the E_1 critical point should be greater than that of the $E_1+\Delta_1$ critical point. However, in LT-GaAs the opposite is observed. Nonetheless the broadening of E_1 with Mn doping is not surprising given the large number of impurities in these samples, and the resulting relaxation of momentum conservation. Assuming Γ follows the trends previously established for doped GaAs,[28] we expect $\Gamma \cong 100$ meV for E_1 and $E_1+\Delta_1$, which should grow with increasing impurity concentration. This is qualitatively consistent with our findings of a combined broadening of 220 meV (see Fig. 5); however a quantitative comparison is not possible due to the uncertainty in carrier and impurity concentrations.

D. $E_{0'}$

The $E_{0'}$ critical point occurs at the zone center as a result of transitions from the heavy and light hole valence bands to the Γ_7 and Γ_8 conduction bands (see Fig. 1). Therefore, the $E_{0'}$ critical point provides insight into changes in the elec-

tronic structure near the zone center. Given our experimental resolution and fitting methods, we determined the shift in $E_{0'}$ to be $\leqslant \pm 20$ meV. Given the strong blueshifting seen in the E_1 critical point (>150 meV), this is quite surprising. Additionally, due to the close proximity of the Mn d^5/d^6 level to the Γ_7 and Γ_8 conduction bands, see Fig. 1, we expect significant blue shifting of $E_{0'}$ from *sp-d* hybridization. The Mn acceptor level is also quite close to the light and heavy hole valence bands at the Γ point. However, this apparent null result, can be explained by a reduction in the strength of $V_{(s,p)d}$ at the zone center. We therefore conclude that the hybridization shifts at the zone center are approximately equal to the strength of the renormalization of the gap from the impurity potentials. It is also interesting to note that the existence of this feature in all Mn doped samples, suggests the the Fermi level is less than 200 meV below the top of the valence band.

The Mn d^5/d^6 level also produces another interesting effect on the derivative spectra of $Ga_{1-x}Mn_xAs$. As mentioned in Sec. III C, samples with $x \geqslant 0.04$ contain an extremely weak extra feature, labeled E_{Mn}, just below $E_{0'}$. Due to the limited amplitude of this component of $d^2\hat{\epsilon}(E)/dE^2$, it is difficult to discuss in detail. However, its origin may be related to a transition from the valence band to the d^5/d^6 level (see Fig. 1). Similar transitions have been observed in $Cd_{1-x}Mn_xTe$ and $Zn_{1-x}Co_xTe$.[16,20] The spectral weight associated with these transitions is generally quite small due to the heavy mass of the *d* level. Additionally this level will generally be split due to the crystal field, thereby broadening the transition.

E. E_2

The E_2 critical point results from the almost parallel nature of the heavy and light hole valence bands and the Γ_6 conduction band near the *X* point (see Fig. 1). We also expect to see shifts in E_2 as a result of the perturbing potential of the impurities. Nonetheless this critical point is clearly unchanged by low-temperature growth and/or Mn doping. This apparent null result for the E_2 critical point may also be explained by the canceling of the impurity and hybridization terms. However, this spectral region is affected by the presence of an oxide layer. Specifically, the additional layer reduces the measured strength of the E_2 critical point, yet it will not affect its position.[27] We therefore attribute the apparent random nature of the strength of this transition seen in Fig. 3 to the presence of the oxide layer, which is not fully accounted for in our model.

Interestingly, both the $E_{0'}$ and E_2 critical points see an enhancement of Θ with increased Mn doping. We believe this results from the additional Coulomb potentials of the impurities in these materials. The potential due to defects in $Ga_{1-x}Mn_xAs$ will be quite complicated since it originates from both acceptors and donors. As discussed in Sec. IV C, it appears that the defects tend to cluster,[38] suggesting they produce dipole or higher order fields. These correlated potentials should be weaker and more complex than the potential of independent impurities, and therefore their effect on the phase of critical points is by no means trivial.

V. SUMMARY AND OUTLOOK

This work is the first ellipsometric study of $Ga_{1-x}Mn_xAs$. In this paper we have detailed the progression of the GaAs band structure upon doping with Mn. The E_1 transition blueshifts with increasing Mn doping, while all other critical points remain unchanged. This blue shifting of E_1 is the result of *p-d* hybridization of the Mn induced impurity band and the GaAs valence band. Therefore, this study demonstrates the existence of the Mn induced impurity band throughout the entire doping range as well as its *d* character. The fact that blueshifting is only seen in the E_1 critical point indicates the strength of V_{pd} is larger in the 111 direction. It is interesting to note that the anisotropy of V_{pd} seen here likely plays a role in the anisotropic magnetoresistance of $Ga_{1-x}Mn_xAs$.[40] The significant increase in broadening of the critical points also establishes the relaxation of the conservation of momentum in these materials. However, $\vec{k}$ still appears to be a good quantum number in this system, as the E_1, $E_{0'}$, and E_2 critical points can all be resolved at every doping level in this study. Additionally the band structure of GaAs appears to remain mostly intact, despite the large number of defects found in these materials. Interestingly, the band-gap renormalization due to defects is compensated by *sp-d* hybridization. Furthermore, these results imply *sp-d* hybridization plays a key role in the optical properties of $Ga_{1-x}Mn_xAs$.

Key insights into the Hamiltonian governing $Ga_{1-x}Mn_xAs$ are clearly provided by this work. Specifically, it is clear that the Mn impurity band plays an important role at all doping levels. Additionally $\vec{k}$ is only partially relaxed in these materials, confirming the assertion that $Ga_{1-x}Mn_xAs$ has the electronic structure of a compound. It is also clear that the impurity potentials are strongly screened in these materials, either by heavy carriers and/or by other impurities. As this is the first ellipsometric study of a compensated semiconductor, it is unclear what role defect correlations play in reducing the perturbation of impurity potentials on the band structure. Therefore further theoretical and experimental evaluation of this problem is clearly called for. However the defects and additional impurity states in these materials result in a large broadening of the critical points. Therefore low temperature measurements are needed to help resolve the exact position of the critical points. Additionally the effect of electron–phonon coupling and potentially the position of d^5/d^6 level could be determined with temperature dependent ellipsometry. Nonetheless this study provides a unique litmus test for further calculations of the $Ga_{1-x}Mn_xAs$ band structure. In fact, one of the reasons the GaAs band structure is so well understood is the large number of calculations based upon and/or compared to experimental determinations of its critical points. We therefore believe these results will be critical in determining the physics governing $Ga_{1-x}Mn_xAs$.

ACKNOWLEDGMENTS

This work was supported by the DOE, NSF, DARPA, ONR, and the F. L. Willis Fund. We are grateful for numerous discussions with L. Cywinski, M. Fogler, A. Fujimori, E. M. Hankiewicz, J. McGuire, L. J. Sham, J. Sinova, and T. Tiwald.

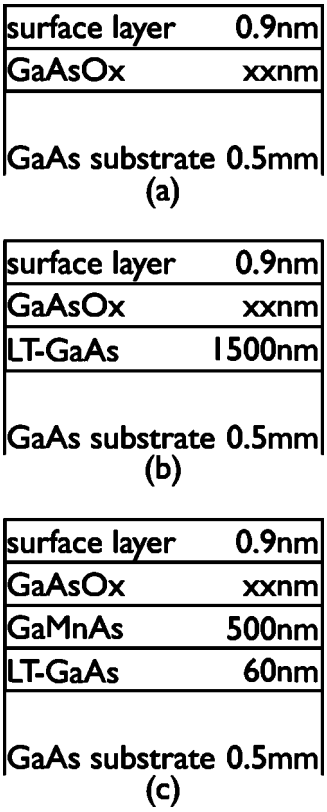

FIG. 7. Schematic diagram of (a) the GaAs substrate model, (b) the model for the LT-GaAs sample, and (c) the $Ga_{1-x}Mn_xAs$ samples.

APPENDIX A: MODELING THE OPTICAL CONSTANTS

As noted in Sec. II, the optical constants cannot be obtained analytically from Ψ and Δ for any of the samples in this study due to surface roughness and the presence of an oxide layer.[34] This problem is compounded by the multilayered nature of the samples. Therefore to obtain the optical constants of the films we have devised a method to properly model these samples. To simplify this problem we first measured Ψ and Δ for a piece of GaAs substrate, which had approximately the same exposure to air and roughening conditions as the other samples in this study. The substrate was successfully modeled with three layers [see Fig. 7(a)]. The first contained the known optical constants of GaAs with a fixed thickness of 0.5 mm. The next two layers were GaAsOx (native oxide), and a surface layer modeling roughness as an effective medium of 50% void and 50% GaAsOx (see Fig. 7).[34,41] We then performed a least-squares fit to Ψ and Δ to determine the oxide and surface layer thicknesses.

Next, we modeled the LT-GaAs data similar to GaAs with an additional 1500 nm thick layer between the substrate and the oxide layer [see Fig. 7(b)]. Initially the thickness of the oxide and surface layers were the same as those determined for the substrate. The optical constants of the LT-GaAs layer were defined using a sum of Lorentzian and Tauc-Lorentzian oscillators:

$$\hat{\epsilon}(E) = \epsilon_0 + \sum_i \hat{\epsilon}_i^{\text{Lorentz}}(E) + \sum_j \hat{\epsilon}_j^{\text{Tauc-Lorentz}}(E), \quad \text{(A1)}$$

$$\hat{\epsilon}_i^{\text{Lorentz}}(E) = \frac{A_i \Gamma_i E_i}{E_i^2 - E^2 - i\Gamma_i E}, \quad \text{(A2)}$$

$$\hat{\epsilon}_j^{\text{Tauc-Lorentz}}(E) = \frac{2}{\pi} P \int_{E_{bi}}^{\infty} \frac{\zeta}{\zeta^2 - E^2} \frac{A_i(\zeta - E_{bi})^2}{(\zeta^2 - E_{ci}^2) + i\Gamma_i^2} d\zeta + i\left[\frac{A_i(E - E_{bi})^2}{(E^2 - E_{ci}^2) + i\Gamma_i^2} \frac{\Theta(E - E_{bi})}{E}\right], \quad \text{(A3)}$$

where $\Theta(E - E_{bi})$ is the unit step function, P implies the Cauchy principle value, and ϵ_0 is a constant used to model the polarizability of the material. Three Lorentzian oscillators were employed to model the effects of one and two phonon absorption in the infrared portion of the spectrum.[42] The Tauc–Lorentzian oscillators, see Eq. (A3), were utilized to model the effect of interband transitions.[43] We note that we choose to model the optical constants using oscillators instead of performing a least-squares fit for $\hat{\epsilon}(E)$ directly so as to ensure the results are Kramers–Kronig consistent. This approach also enabled us to improve upon standard techniques by including transmission data and the effect of oscillators centered below the ellipsometer's range. Lastly, we note that for $0.62\ \text{eV} \leqslant E \leqslant 1.42\ \text{eV}$ this procedure produced optical constants consistent (within 1%) with previous results derived from a combination of normal incidence transmission and reflection.[13,44]

To obtain the initial conditions for the LT-GaAs generic layer, we first fit the optical constants of GaAs using Eq. (A1). We then applied this model to the LT-GaAs data and performed a fit for the thicknesses of the LT-GaAs, oxide, and surface layers. Next we fit for the parameters of each oscillator separately. This was done to avoid the effect of correlations due to the large overlap of the oscillators. Once all the oscillators had been fit, we refit the thickness of each layer. This iterative method was performed until the fit could no longer be improved. We repeated the fitting procedure

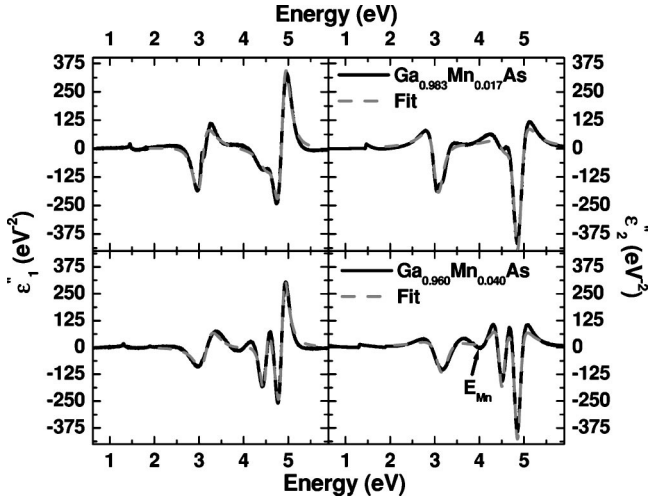

FIG. 8. Two representative fits of $d^2\epsilon(E)/dE^2$. In the bottom panel the extra feature at $E \approx 4.0$ eV can be seen, however it is too weak to provide a reliable fit.

with a number of different initial conditions so as to ensure the final answer was not dependent on our original values.

The $Ga_{0.983}Mn_{0.017}As$ data was fit after the LT-GaAs sample, using a similar approach, however the model now contained a 500 nm $Ga_{0.983}Mn_{0.017}As$ layer atop a 60 nm LT-GaAs layer (see Fig. 7). Since the penetration depth for most of the fitted range was less than 500 nm, the thickness of the LT-GaAs layer was never allowed to vary due to its weak contribution to the data. The remaining $Ga_{1-x}Mn_xAs$ samples were fit in a similar fashion, however they contained two additional oscillators. We first modeled the effect of free carriers using the Drude form (a Lorentzian with $E_i=0$), and next we added an additional Tauc–Lorentzian oscillator to model the effect of interband transitions from the GaAs valence band to the Mn induced impurity band.

APPENDIX B: FITTING THE DERIVATIVE SPECTRA

Two representative plots of the $d^2\hat{\epsilon}(E)/dE^2$ spectra generated by least-squares fitting are compared to the experimental results in Fig. 8. We started the 2D line shape analysis with GaAs and LT-GaAs. In GaAs and LT-GaAs the E_1 and $E_1+\Delta_1$ critical points were fit simultaneously assuming a constant spin orbit splitting ($\Delta_1=0.224$ eV). The $E_{0'}$ and E_2 critical points were also fit together, however constant separation between the two was not assumed.[24] Since we were unable to distinguish the $E_1+\Delta_1$ critical point from E_1 in the $Ga_{0.983}Mn_{0.017}As$ sample, we fit the data in the region of the E_1 critical point with a single 2D line shape. For the remaining Mn samples the broadening of E_1 was large enough that it affected the $E_{0'}$ fit. Therefore, for the samples with $x \geqslant 0.028$, the E_1, $E_{0'}$, and E_2 critical points were fit simultaneously. Lastly, as discussed earlier, for samples with $x \geqslant 0.04$ an additional feature could be seen in the derivative spectra (labeled E_{Mn}). Therefore in these samples four peaks were fit simultaneously, improving the quality of the fit. As seen in Fig. 8, this unfortunately does not provide a good match to this extra peak, therefore the parameters determined for this extra peak are not reported.

*Electronic address: burch@physics.ucsd.edu
†Permanent address: Department of Physics, University of California, Riverside, CA 92521.

[1] H. Ohno, Science **281**, 951 (1998); H. Ohno, A. Shen, F. Matsukura, A. Oiwa, A. Endo, S. Katsumoto, and Y. Iye, Appl. Phys. Lett. **69**, 363 (1996).
[2] S. A. Wolf, D. D. Awschalom, R. A. Buhrman, J. M. Daughton, S. von Molnar, M. L. Roukes, A. Y. Chtchelkanova, and D. M. Treger, Science **294**, 1488 (2001).
[3] T. Dietl, Semicond. Sci. Technol. **17**, 377 (2002).
[4] G. Alvarez and E. Dagotto, Phys. Rev. B **68**, 045202 (2003).
[5] M. Berciu and R. N. Bhatt, cond-mat/0111045 (2001).
[6] A. Chattopadhyay, S. Das Sarma, and A. J. Millis, Phys. Rev. Lett. **87**, 227202 (2001).
[7] E. M. Hankiewicz, T. Jungwirth, T. Dietl, C. Timm, and J. Sinova, cond-mat/0402661 (2004).
[8] S. R. Eric Yang and A. H. MacDonald, Phys. Rev. B **67**, 155202 (2003).
[9] R. A. Chapman and W. G. Hutchinson, Phys. Rev. Lett. **18**, 443 (1967); M. Linnarsson, E. Janzen, B. Monemar, M. Kleverman, and A. Thilderkvist, Phys. Rev. B **55**, 6938 (1997).
[10] G. Mahieu, P. Condette, B. Grandidier, J. P. Nys, G. Allan, D. Stievenard, Ph. Ebert, H. Shimizu, and M. Tanaka, Appl. Phys. Lett. **82**, 712 (2002); T. Tsuruoka, N. Tachikawa, S. Ushioda, F. Matsukura, K. Takamura, and H. Ohno, *ibid.* **81**, 2800 (2002).
[11] H. Asklund *et al.*, Phys. Rev. B **66**, 115319 (2002).
[12] O. Rader, C. Pampuch, A. M. Shikin, W. Gudat, J. Okabayashi, T. Mizokawa, A. Fujimori, T. Hayashi, M. Tanaka, A. Tanaka, and A. Kimura, Phys. Rev. B **69**, 075202 (2004); J. Okabayashi, A. Kimura, O. Rader, T. Mizokawa, A. Fujimori, T. Hayashi, and M. Tanaka, Physica E (Amsterdam) **10**, 192 (2001).
[13] E. J. Singley, R. K. Kawakami, D. D. Awschalom, and D. N. Basov, Phys. Rev. Lett. **89**, 097203 (2002); E. J. Singley, K. S. Burch, J. Stephens, R. K. Kawakami, D. D. Awschalom, and D. N. Basov, Phys. Rev. B **68**, 165204 (2003).
[14] K. S. Burch, E. J. Singley, J. Stephens, R. K. Kawakami, D. D. Awschalom, and D. N. Basov, Phys. Rev. B (submitted).
[15] P. Y. Yu and M. Cardona, *Fundamentals of Semiconductors* (Springer, Berlin, 1996).
[16] Y. D. Kim, S. L. Cooper, M. V. Klein, and B. T. Jonker, Phys. Rev. B **49**, 1732 (1994).
[17] F. C. Zhang and T. M. Rice, Phys. Rev. B **37**, 3759 (1988); T. Dietl, F. Matsukura, and H. Ohno, cond-mat/0109245.
[18] J. Blinowski, P. Kacman, and T. Dietl, cond-mat/0201012 (2002).
[19] P. M. Hui, H. Ehrenreich, and K. C. Hass, Phys. Rev. B **40**, 12346 (1989).
[20] P. Lautenschlager, S. Logothetidis, L. Via, and M. Cardona, Phys. Rev. B **32**, 3811 (1985).
[21] Y. D. Kim, Yia Chung Chang, and M. V. Klein, Phys. Rev. B **48**, 17770 (1993).
[22] R. M. A. Azzam and N. M. Bashara, *Ellipsometry and Polarized Light* (North-Holland, Amsterdam, 1977).
[23] We note that we have assumed the magnetic response is negligible, i.e., $\mu=1$.
[24] P. Lautenschlager, M. Garriga, S. Logothetidis, and M. Cardona, Phys. Rev. B **35**, 9174 (1987).
[25] We note that intereference resulting from reflection off of the back of the substrate is possible. However these generally are incoherent and consequently the reliability of the model is reduced. Therefore we have developed a technique to roughen the back surface of the substrate without damaging the films to prevent this interference from occurring.
[26] J. Humlicek, M. Garriga, M. I. Alonso, and M. Cardona, J. Appl. Phys. **65**, 2827 (1989).
[27] D. E. Aspnes and A. A. Studna, Phys. Rev. B **27**, 985 (1983).
[28] F. Lukes, S. Gopalan, and M. Cardona, Phys. Rev. B **47**, 7071 (1993).
[29] J. E. Rower and D. E. Aspnes, Phys. Rev. Lett. **25**, 162 (1970).
[30] R. B. Bylsma, W. M. Becker, J. Kossut, U. Debska, and D. Yoder Short, Phys. Rev. B **33**, 8207 (1986).

[31] H. Lee, T. D. Kang, Y. J. Park, H. T. Oh, H. Y. Cho, R. Moriya, and H. Munekata, J. Korean Phys. Soc. **42**, S441 (2003).
[32] L. Vina and M. Cardona, Phys. Rev. B **29**, 6739 (1984).
[33] L. Vina and M. Cardona, Phys. Rev. B **34**, 2586 (1986).
[34] M. Erman, J. B. Theeten, P. Chambon, S. M. Kelso, and D. E. Aspnes, J. Appl. Phys. **56**, 2664 (1984).
[35] M. J. Seong, S. H. Chun, H. M. Cheong, N. Samarth, and A. Mascarenhas, Phys. Rev. B **66**, 033202 (2002); K. M. Yu, W. Walukiewicz, T. Wojtowicz, W. L. Lim, X. Liu, Y. Sasaki, M. Dobrowolska, and J. K. Furdyna, Appl. Phys. Lett. **81**, 844 (2002); R. Moriya and H. Munekata, J. Appl. Phys. **93**, 4603 (2003).
[36] A. vanEsch, L. Van Bockstal, J. De Boeck, G. Verbanck, A. S. van Steenbergen, P. J. Wellmann, B. Grietens, R. Bogaerts, F. Herlach, and G. Borghs, Phys. Rev. B **56**, 13103 (1997).
[37] N. Suzuki, M. Shirai, T. Ogawa, and I. Kitagawa, J. Magn. Magn. Mater. **177-181**, 1383 (1998); J. H. Park, S. K. Kwon, and B. I. Min, Physica B **281**, 703 (2000); J. Inoue, S. Nonoyama, and H. Itoh, Phys. Rev. Lett. **85**, 4610 (2000); L. M. Sandratskii and P. Bruno, Phys. Rev. B **66**, 134435 (2002); E. Kulatov, H. Nakayama, H. Mariette, H. Ohta, and Yu. A. Uspenskii, *ibid.* **66**, 045203 (2002); M. Jain, L. Kronik, J. R. Chelikowsky, and V. V. Godlevsky, Phys. Rev. B **64**, 245205 (2001); P. Mahadevan and A. Zunger, cond-mat/0309509 (2003); S. Sanvito, P. Ordejn, and N. A. Hill, Phys. Rev. B **63**, 165206 (2001).
[38] J. M. Sullivan, G. I. Boishin, L. J. Whitman, A. T. Hanbicki, B. T. Jonker, and S. C. Erwin, Phys. Rev. B **68**, 235324 (2003); C. Timm, F. Schfer, and F. von Oppen, Phys. Rev. Lett. **89**, 137201 (2002).
[39] M. Chandrasekhar and F. H. Pollak, Appl. Phys. Lett. **15**, 2127 (1977); G. Leibiger, V. Gottschalch, B. Rheinlander, J. Sik, and M. Schubert, *ibid.* **77**, 1650 (2000).
[40] K. Hamaya, T. Taniyama, R. Moriya, and H. Munekata, J. Appl. Phys. **94**, 7657 (2003); D. V. Baxter, D. Ruzmetov, J. Scherschligt, Y. Sasaki, X. Liu, J. K. Furdyna, and C. H. Mielke, Phys. Rev. B **65**, 212407 (2002); M. Abolfath, T. Jungwirth, J. Brum, and A. H. MacDonald, *ibid.* **63**, 054418 (2001); T. Dietl, H. Ohno, F. Matsukura, J. Cibert, and D. Ferrand, Science **287**, 1019 (2000).
[41] G. E. Jellison, L. A. Boatner, D. H. Lowndes, R. A. McKee, and M. Godbole, Appl. Opt. **33**, 6053 (1994).
[42] F. Wooten, *Optical Properties of Solids* (Academic, New York, 1972).
[43] G. E. Jellison, Jr. and F. A. Modine, Appl. Phys. Lett. **69**, 371 (1996).
[44] I. Kuryliszyn-Kudelska, J. Z. Domagala, T. Wojtowicza, X. Liu, E. Lusakowska, and W. Dobrowolski, J. Appl. Phys. **95**, 603 (2004).